Mineralogy and structures below Deccan Traps: Evidences from scientific drilling in the Koyna seismogenic zone, India

Surajit Misra[1,2,*] ⓘ, Deepjyoti Goswami[1] and Sukanta Roy[1]

[1]*Ministry of Earth Sciences, Borehole Geophysics Research Laboratory, Karad, Maharashtra 415 105, India.*
[2]*Present address: Department of Geological Sciences, Gauhati University, Guwahati, Assam 781 014, India.*
*Corresponding author. e-mail: misrasurajit@gmail.com

We study the deformation features preserved in basement granitoids recovered by scientific core drilling from an active seismic zone in the Koyna region, Deccan Traps, India. The region is characterized by recurrent reservoir triggered seismicity for the past 55 years, including the 1967 M6.3 Koyna earthquake, which produced the Donichawadi fissure zone. We investigate the basement granitoids down to a depth of 1.5 km in a set of four boreholes. Salient findings are as follows: (1) Basement rocks are composed of granite, granite-gneiss and migmatitic gneiss, characterized by greenschist to amphibolite facies metamorphism, (2) Distinctive brittle deformation features, such as fault breccias, fault gouge, prominent slickenlines and slickensides on fractures and pseudotachylites indicate proximity to a fault zone, (3) Fault zones are enriched with secondary precipitations of ferruginous and calcium-rich material which are the evidences of fluid-filled fractures at depth, (4) Fault breccia and gouge are preserved along with intense shattering of cores in zones of near-vertical fractures. Combined with information from downhole geophysical logs in a 3 km deep scientific borehole and the distribution of hypocentres, the study provides strong constraints for the subsurface extension of the Donichawadi fissure zone that is active to this day. The new datasets provide evidence for multiple episodes of fracturing and fault rock formation in an intraplate, near-vertical, fault zone and chemical changes of the fault rocks in the presence of water at seismogenic depth.

Keywords. Koyna seismogenic zone; Deccan Traps; granitic basement; scientific drilling; fault zone; brittle deformation.

1. Introduction

Intraplate earthquakes occur in the plate interior but are possibly driven by plate boundary forces (Wdowinski 1998 and references therein). A component of the net forces acting in the plate boundary may be transferred towards the plate interior, which slowly deforms the intraplate region (Zoback *et al.* 1989). However, local structural heterogeneities generally play a significant role to re-distribute this strain. Several hundred to thousands of years are required to accumulate high stress in intraplate regions in order to generate a large magnitude earthquake (Kanamori and Brodsky 2004). However, in the last two to three decades, certain areas within the intraplate or

tectonically stable regions have experienced rapid increases in seismicity due to anthropogenic activities such as mining, construction of large gravity dams, injection of fluid into the subsurface to increase formation permeability, and injection of water for enhanced geothermal systems (McGarr *et al.* 2002 and references therein). It is seen that such activities significantly alter the pre-existing subsurface conditions in multiple ways, e.g., by increasing pore fluid pressure in the fault zone, by reducing frictional strength through chemical alteration and other mechanisms (Sibson 1974, 1977a, b). As a result, earthquake nucleates in pre-existing fault(s)/fractures well before the normal or expected recurrence time. Study of the subsurface stress regime, rate of deformation of the crust, localised zone(s) of high-stress concentration, etc., are essential to understand the seismic potential of such regions. In addition, study of the deformation features, microstructural variations preserved in rocks during earthquakes, composition and properties of fault zone materials and pseudotachylites may provide critical constraints in understanding the mechanics of earthquake and faulting processes. Structural analysis of the intact host rock and the fault zone rocks may provide new insights into the subsurface kinematics of the region.

Scientific drilling along active faults provide rare opportunities to sample fault core and to study the internal structure and deformation mechanism(s) of the fault zone (Reches and Ito 2007). In recent times, scientific drilling has been carried out in a number of active faults worldwide, e.g., San Andreas Fault Zone Observatory at Depth (SAFOD), Taiwan Chelungpu Fault Drilling Project (TCDP), Nojima Fault drilling in SW Japan, Deep Fault Drilling Project (DFDP) in the Alpine Fault in New Zealand and Gulf of Corinth in Greece. These scientific drilling programmes have brought forth valuable information on deep fault zone rocks from studies on recovered core samples (Ando 2001; Lin *et al.* 2001; Ma *et al.* 2006; Schleicher *et al.* 2006; Bradbury *et al.* 2007; Yeh *et al.* 2007; Zoback 2007; Wu *et al.* 2008; Louis *et al.* 2008; Lockner *et al.* 2009; Zoback *et al.* 2010; Holdsworth *et al.* 2011; Boullier 2011; Taylor *et al.* 2011; Carpenter *et al.* 2012; Sutherland *et al.* 2012; Townend *et al.* 2013; Warr *et al.* 2014; Toy *et al.* 2015, 2017; Allen *et al.* 2017). However, the delineation of the subsurface fault zones and acquisition of cores from the fault zone(s) and their surrounding host rocks are often quite complicated.

Geophysical well-logging plays an important role in the characterization of fault damage zones at depth. Generally, physical and mechanical properties of fault zone rocks are significantly different from the intact host rock formation. Measurements in multiple scientific boreholes have shown that fault zones are generally characterised by low density, low resistivity, low P- and S-wave velocities, high porosity, high Poisson's ratio and low Young's modulus (Ben-Zion and Sammis 2003; Boness and Zoback 2004; Hickman and Zoback 2004; Ito and Kiguchi 2005; Faulkner *et al.* 2006; Ikari *et al.* 2009; Carpenter *et al.* 2009, 2014; Jeppson *et al.* 2010; Zoback *et al.* 2011; Townend *et al.* 2013; Jeppson and Tobin 2015; Allen *et al.* 2017; Goswami *et al.* 2019). Additionally, in many cases, significant rotation in subsurface stress orientation is observed in proximity to the fault damage zones (Barton and Zoback 1994; Brudy *et al.* 1997; Wu *et al.* 2007; Lin *et al.* 2010; Goswami *et al.* 2020). Therefore, downhole geophysical measurements provide important information for distinguishing between fault damage zones and the surrounding intact host rocks, which may provide a basis for sidewall coring and/or supporting further critical investigations on the cores/cuttings obtained from such zones of anomalous rock properties (Misra *et al.* 2017; Goswami *et al.* 2020). Additionally, modern high-resolution borehole image logs provide critical information about the orientation of subsurface structural features that could not be obtained otherwise from cores, as in most cases, cores are generally not oriented or cores are missing due to poor recovery in highly fractured zones.

Cores/cuttings retrieved through scientific drilling from seismogenic depths provide valuable information about the composition, texture, internal structure, fracture patterns, deformation mechanism of the fault zone rocks, which play an important role in controlling fault movements and also explaining the role of fluids in activating pre-existing faults (Evans and Chester 1995; Caine *et al.* 1996; Evans *et al.* 1997; Vrolijk *et al.* 1999; Faulkner and Rutter 2003; Wibberley *et al.* 2008; Bradbury *et al.* 2015). For example, fault zone materials from SAFOD reveal that fault rocks are comprised of serpentinite-bearing clay gouge of low frictional strength, which is responsible for active creeping in a $\sim$200 km long section of the San Andreas Fault and also explains the long-lasting debate on the stress-heat flow paradox (Lachenbruch and Sass 1980; Hickman and Zoback 2004;

Scholz *et al.* 2006; Lockner *et al.* 2011; Bradbury *et al.* 2011). Detailed geological analyses indicate that the amorphous materials observed in the gouge is a result of comminution of grains due to active creeping and authigenic clay growth, not of melt origin (Janssen *et al.* 2014). On the other hand, the Chelungpu fault zone contains fault breccias and pseudotachylites (Ma *et al.* 1999, 2001; Yeh *et al.* 2007). Unlike SAFOD, the amorphous materials present in the clay gouge of the principal slip zone (PSZ) of Chelungpu fault are of melt origin, formed by a rise in temperature during seismic slip (Janssen *et al.* 2014). On the other hand, mineralogical and structural analysis of fault core in the Alpine Fault (DFDP) reveals PSZ gouge and cataclasite-series of rocks formed due to elastico-frictional deformation within the fault zone (Toy *et al.* 2015). Sutherland *et al.* (2012) provided a detailed account of the formations of cataclasites and mylonites in the presence of fluids within the fault zone. Thus, mineralogical and structural studies of fault zone rocks from different regions help in characterizing the internal structure of the fault zones and mechanism of earthquake genesis in a region.

The Koyna seismogenic zone in the Deccan trap province, western India (figure 1), characterized by shallow and recurrent water-reservoir triggered seismicity during the past five decades, provides an excellent site to study potential brittle deformation in Archean granitoids through scientific drilling. Since the impoundment of the Koyna reservoir in 1962, the region has experienced the largest triggered earthquake of magnitude $M \sim 6.3$ in 1967, 22 earthquakes of magnitude $5.0 \geq M \geq 5.9$, more than 200 earthquakes of magnitude $M \geq 3.5$ and several thousand smaller earthquakes (Gupta 1992, 2002, 2011; Gupta *et al.* 2015, 2016). The seismic activity was enhanced after the impoundment of the Warna Reservoir, located ~ 20 km to the south of Koyna Dam. Notable features constrained from seismological studies are as follows: (i) the entire seismic activity is restricted within a relatively small volume, covering an area of ~ 20 km $\times$ 30 km to the south of the Koyna Dam and extending southward to the vicinity of the Warna Dam, (ii) seismicity extends to a depth of ~ 10 km, with the great majority of the earthquakes in depth range 2–8 km, (iii) earthquake hypocentres are located in the granitic basement rocks underlying the Deccan basalt, and (iv) the frequency of earthquakes is modulated by the changes in the water levels of the Koyna and Warna reservoirs,

particularly during the monsoon and post-monsoon seasons (Gupta 1992, 2002; Talwani 1997a, b; Gupta *et al.* 2015). The 1967 $M \sim 6.3$ earthquake formed a NNE–SSW trending surface rupture zone, known as the Donichawadi fissure zone, and mapped a few km southeastward of the Koyna Dam along a length of ~ 4 km and width of ~ 200 m (GSI 1968; Misra *et al.* 2017). Recent seismological studies show a concentration of seismicity along the trend of the fissure zone (Gupta *et al.* 2017; Shashidhar *et al.* 2017). Since earthquakes occur predominantly in the granitic basement rock, detailed investigations on basement rock samples may provide valuable insights for understanding subsurface processes associated with the recurrent seismicity in the region.

In the present study, we carry out geological investigations on the core samples of intact as well as fault zone rocks recovered from depths down to 1.5 km in the granitic basement through scientific drilling at four sites in the Koyna seismogenic zone. Based on our investigations, we report: (i) the mineralogical and structural features of the basement granitoids and deformation sequences for the first time, (ii) signatures of brittle deformation and their possible association with recurrent seismic activity at depth, (iii) composition of chemically altered fault zone rocks, (iv) evidence of fluid channelization at depth, and (v) fractures and their relationship with the pre-existing anisotropy, and discuss the implications of the acquired data towards better understanding of the recurrent triggered earthquakes in the region.

2. Geologic setup

The rocks exposed in Koyna and the surrounding region of western India consist of Deccan flood basalts that erupted as a consequence of the passage of Indian plate over the Reunion hotspot about 65 my ago (Morgan 1972; Cox and Hawkesworth 1985; Beane *et al.* 1986; Courtillot *et al.* 1986). Duncan and Pyle (1988) and Courtillot *et al.* (1986) suggested a narrow span of ~ 1 my for the eruption of the lavas with a mean age of 65 Ma. However, other studies have reported a larger time span of a few million years for the volcanism (Venkatesan *et al.* 1986; Courtillot *et al.* 1988). Typically, the flood basalt formation comprises a thick succession of lava flows, with the individual flows varying in thickness from a few metres to several tens of metres. The Deccan flood basalts
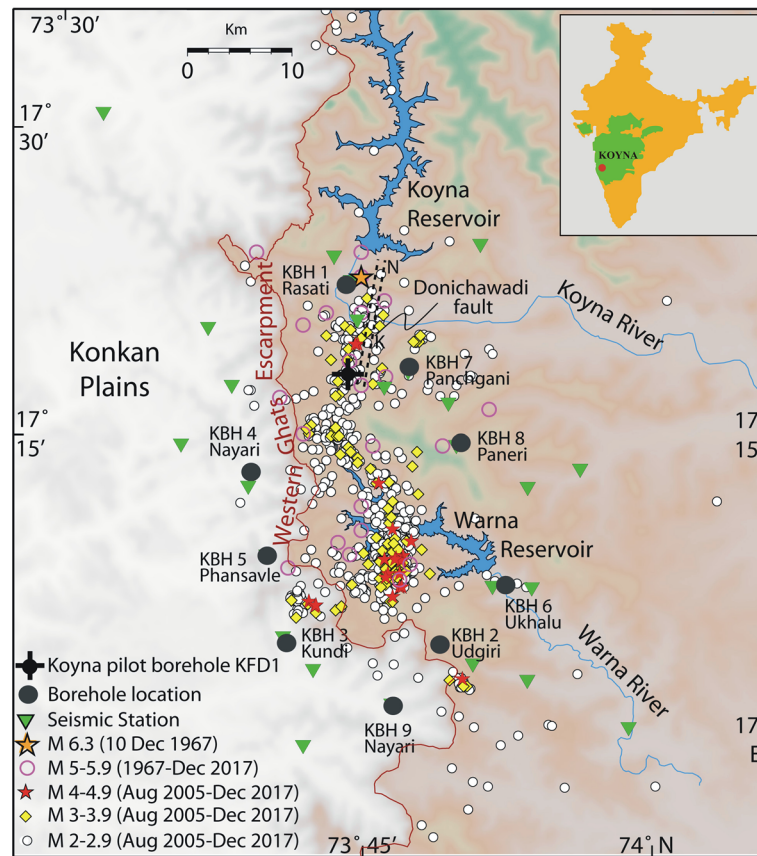
Figure 1. Map of Koyna seismogenic zone showing the distribution of cored boreholes KBH-1 through KBH-9 and borehole KFD1. The seismicity data, taken from Shashidhar *et al.* (2017) is also plotted. The Koyna (Shivajisagar) and Warna artificial water reservoirs and the trace of the Donichawadi Fault are also shown. The Western Ghats escarpment divides the region into a low-lying western part called the Konkan coastal plains (light shaded region) and an elevated region in the eastern part (dark shaded region). Inset shows the location of Koyna in the Deccan Traps province (shaded green) on the outline map of India.

exposed in different parts of western and central India have been studied extensively to characterize the lava flows from geological, geochemical and geochronological aspects (Cox and Hawkesworth 1985; Beane *et al.* 1986; Devey and Lightfoot 1986; Venkatesan *et al.* 1986; Duncan and Pyle 1988; Khadri *et al.* 1988; Mahoney 1988; Mitchell and Widdowson 1991; Seth 1999, 2007). However, the thickness of the Deccan Traps and the characteristics of the underlying basement rocks have remained a subject of debate due to the lack of deep drilling in the region. The thickness of the Deccan Traps is believed to vary from a few thousand metres in the western parts to a few tens of metres in the eastern parts of the flood basalt province. Drilling through the Deccan Traps at Killari, near the southeastern margin of the province, revealed a trap thickness of 338 m (Gupta and Dwivedy 1996). In contrast, continuous vertical successions of basaltic flows with thickness of more than 1200 m are observed along some road sections in the Western Ghats (Bondre *et al.* 2004). The Mahad–Mahabaleshwar section in the Western Ghats provides a relatively uniform, undeformed flood basalt sequence. Najafi *et al.* (1981) have reported 47 flows of Deccan Traps forming a 1240 m thick horizontal sequence along this section. Geophysical studies carried out during the past few decades have also attempted to characterise the thickness of Deccan Traps. On the basis of deep resistivity sounding data collected along Solapur–Karad–Guhagar traverse, Kailasam *et al.* (1976) inferred the thickness of the Deccan Traps in the range 370–1000 m. Deep seismic sounding studies carried out along a profile from Guhagar on the west coast to Chorochi in the east and passing through Koyna and Karad revealed variations in the thickness of the Deccan trap from 0.4 km in the east to 1.5 km near the west coast (Kaila *et al.* 1981). Trap thickness was interpreted to be ∼0.4 km near Chorochi, ∼0.6 km near Karad, 1–1.1 km near Koyna and then decreasing to ∼0.7 km

between Alore and Chiplun. However, information on the rock formations below the Deccan Traps was meager, limited to interpretations from geophysical data only.

Scientific drilling studies in the Koyna region, undertaken by the Ministry of Earth Sciences, India, in 2012, provide a rare opportunity to gain access to the entire thickness of Deccan flood basalt formation and the underlying basement rocks. Vertical core drilling was carried out at nine sites in the vicinity of the Koyna seismogenic zone during the preparatory phase of investigations to study the reservoir-triggered seismicity in the region. The borehole sites are located along the periphery of the seismogenic zone, extending from Rasati (close to the Koyna Dam) in the north to Udgiri (south of the Warna Reservoir) in the south and cover both eastern and western parts of the Western Ghats escarpment (figure 1). The first direct information on trap thickness in this region was obtained from borehole KBH-1 at Rasati, near Koyna where the thickness was found to be 932.5 m (Roy *et al.* 2013). All the nine boreholes penetrated the Deccan basaltic pile and continued a few hundred metres into the underlying granitic basement (Gupta *et al.* 2017). Preliminary studies on the core samples of Deccan basalt formation, including the physical characteristics of the lava flows, were reported from two boreholes KBH-1 and KBH-7 by Sinha *et al.* (2017) and Misra *et al.* (2017), and information on the rock types comprising the basement granitoids from four boreholes KBH-1, KBH-5, KBH-6 and KBH-7 were reported by Misra *et al.* (2017). The cores reveal a relatively sharp contact between Deccan basalt formation and the granitic basement, with the contact zone devoid of infra-trappean sediments but consisting of less than a meter to a few meters thickness of rock representing a mish-mash resulting from the contact of hot lava flows emplaced over the uppermost weathered portions of the granitic basement. The thickness of Deccan Traps in the Koyna seismogenic zone is found to vary in the range of 412–1251 m. The boreholes to the west of the Western Ghats escarpment reveal trap thicknesses in the range of 412–518 m, in contrast to the boreholes on the eastern side, which show significantly larger thicknesses, 775–1251 m. In spite of the large surface relief (order 1000 m) and the significant variations in trap thickness, the undulations in the basement topography are relatively small, generally within 100 m. The basalt-basement contact is relatively sharp, characterized by cohesive material intermixed with clasts of both basalt and granite within dark-coloured ferruginous cement. The contact zones in individual boreholes vary in thickness, 2 m in KBH-1, 45 cm in KBH-5, 11 m in KBH-6 and 90 cm in KBH-7.

The basement cores from boreholes KBH-1, KBH-5, KBH-6 and KBH-7, recovered from the northern, western, southern and eastern parts of the study region, respectively, are considered as representative of the basement granitoids in the Koyna seismogenic zone. Also, these boreholes provide access to substantial thickness of the basement granitoids, 588, 406, 715 and 251 m, respectively. The location, total vertical depth, and thicknesses of Deccan basalt and granitic basement in the individual boreholes are listed in table 1. Lithologs prepared from the study on cores show the spatial variations in composition of the granitoids in the region (figure 2). In general, the basement rocks are composed of granite, granite-gneiss and migmatitic gneiss with localised occurrences of amphibolites. Mesoscopic and microscopic studies have shown that the basement section represented in borehole KBH-1 is dominantly composed of granite gneiss ($\sim$60%), migmatitic gneiss ($\sim$25%), granite ($\sim$10%), amphibolite and other mafics ($\sim$5%). Granites exhibit prominent igneous textures with interlocking arrangement between grains. Granite-gneisses show well developed gneissosity in most cases (figure 3a). The basement section represented in borehole KBH-5 is dominantly composed of migmatitic gneiss including amphibolite ($\sim$65%), granite gneiss ($\sim$25%), and granite ($\sim$10%). Prominent ductile deformation bandings are present within the gneisses (figure 3b). The basement section represented in borehole KBH-6 is dominantly composed of granite ($\sim$55%), amphibolite and other mafics ($\sim$20%), granite gneiss ($\sim$15%), and migmatitic gneiss ($\sim$10%). Prominent deformation bandings are found in granite gneisses (figure 3c). The basement section represented in borehole KBH-7 is dominantly composed of migmatitic gneiss ($\sim$60%), granite gneiss ($\sim$20%), granite ($\sim$15%), amphibolite and mafic dyke ($\sim$5%). Igneous textures are predominantly present within these granites and granite gneisses (figure 3d).

This scientific drilling has also established that the $\sim$65 Ma Deccan flood basalt lies directly over a Precambrian granite-gneiss basement. U–Pb dating of zircons from a granodiorite sample from

Table 1. *List of boreholes of the present study, along with the thicknesses of basalt and granitic basement rock as observed from studies on core samples.*

Borehole designation (location)	Latitude, longitude, elevation (masl)	Total vertical depth (m)	Depth to base of Deccan basalt (w.r.t. borehole collar elevation) (m)	Depth to base of Deccan basalt (w.r.t. mean sea level) (m)	Granitic basement section	
					Start depth (m)	End depth (m)
KBH1 (Rasati)	17°22′38.5″N 73°44′27.8″E 580 m	1522.5	932.50	−352.50	934.50	1522.5
KBH5 (Phansavle)	17°09′1.2″N 73°40′2.6″E 131 m	906.5	499.70	−368.70	500.15	906.5
KBH6 (Ukhalu)	17°07′33.1″N 73°52′8.8″E 570 m	1500.7	775.04	−205.04	786.04	1500.7
KBH7 (Panchgani)	17°18′07″N 73°47′28.2″E 960 m	1503.0	1251.23	−291.23	1252.13	1503.0

999 m depth representing the TTG composition and a monzogranite sample from 958 m depth in the borehole KBH-1 yield ages of 2710±63 Ma and 2700±49 Ma, respectively (Rao *et al.* 2017). Hf isotopic data indicate their emplacement as crust building juvenile magma at ∼2700 Ma.

3. Faults and fractures in the basement

Seismic slip along a fault surface causes brittle deformations and highly fractured rocks. The fracture density generally decreases with distance away from the fault core or principal slip zone (Sibson 1986; Paschier and Trouw 2005). Fault core or principal slip zone is frequently surrounded by a highly fractured fault damage zone. Due to progressive seismic activities, fractures generally extend along length and width based on the energy released during an earthquake. These fractures are commonly restricted within a particular zone, identified here as fault zone.

Brittle deformation features of varying intensity are well preserved in the basement granitoids of the Koyna region. To identify the fault zones in the core and provide a better representation of the intensity of brittle deformation, we propose a scale of deformation termed as Sample Quality Designation (SQD). The SQD classification is primarily based on the length of available core samples, which is shown in figure 4. Cores are classified into four categories: Category-A for core length >50 cm, Category-B for 25–49 cm, Category-C for 5–24 cm and Category-D for <5 cm. Physical observations on cores suggest a gradual increase in fracture density from SQD A to SQD D. Core samples from SQD A and B are highly intact and show comparatively lower fracture density than SQD C and D. SQD C and D are considered as highly fractured zones and may be associated with fault damage zones. The SQD generally agrees with the Rock Quality Designation (RQD) (Misra *et al.* 2017) and therefore provides additional constraints to delineate the extension of fault zones in the Koyna seismogenic zone. The changes in SQD of the basement granitoids with depth are indicated along with the lithologs of boreholes KBH-1, KBH-5, KBH-6 and KBH-7 (figure 2). Thus, SQD helps to classify core samples based on the intensity of brittle deformation and fracture density.

The depth sections in the basement granitods with SQD C and D in the KBH-1, KBH-5, KBH-6 and KBH-7 cores correspond to zones of intensive faulting and fracturing (figure 2). The fractures in all the four boreholes show dominant dip angles in a narrow range, 30°–45° with the vertical borehole axis. Intensity of fracturing varies both within individual boreholes as well as between different boreholes. Both shear and extensional fractures are preserved in these core sections. Fractures are
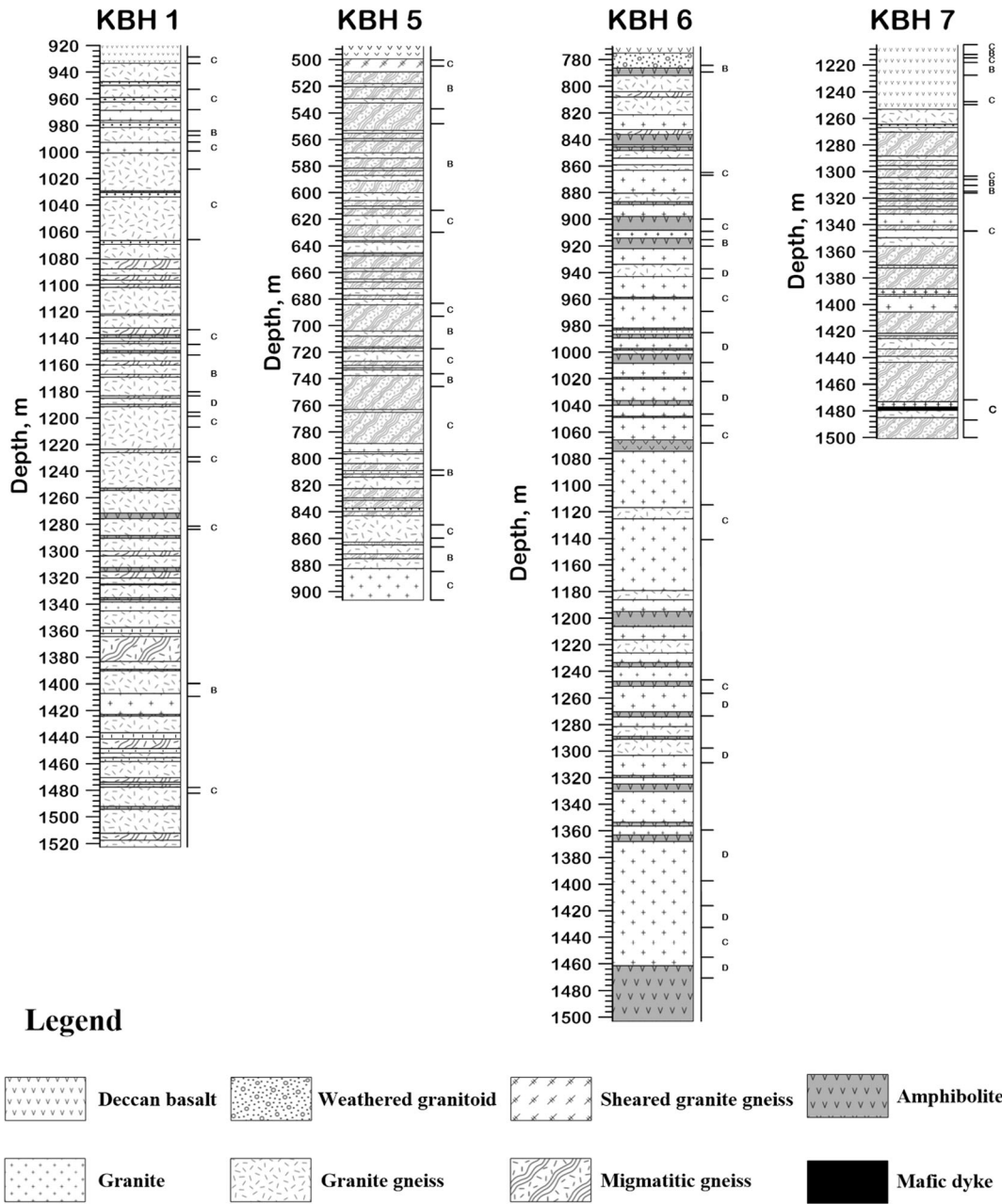
Figure 2. Lithologs prepared from cores of granitic basement section in boreholes KBH-1, KBH-5, KBH-6 and KBH-7. These lithologs represent the variation in basement rock types in the Koyna seismogenic zone. Major rock types are granite, granite gneiss and migmatitic gneisses. In borehole KBH-7, a mafic dyke body that cross-cuts the basement section has been observed. Depth intervals marked as A, B, C and D represent the scale of deformation (SQD), with C and D representing the fault zones within the basement cores.

characterized by displacement of pre-existing features and secondary precipitations. Most fractures are fissures (Mode-I) and/or shear fractures (Mode-II). Fractures are interconnected and form an anastomosing network, which may facilitate fluid flow at depth. Secondary mineralization, silicification, cementation and reddish-brown iron staining are commonly found within SQD C and D zones (figures 5i and 6a, b).

4. Mineralogy, microstructures and deformation sequence

The basement granitoids are dominantly composed of granites, granite-gneiss and migmatitic gneisses. Structural investigations of these cores reveal both the ductile and brittle deformation features, which are represented here as D_1, D_2 and D_3. The D_1, D_2 and D_3 deformation events are characterized on the

Figure 3. Photographs of borehole core samples from the Koyna seismogenic zone showing the sharp contacts between Deccan basalt and granitic basement rock at different sites and deformation signatures of ductile and brittle nature preserved in the granitic basement rock. **(a)** Core sample from KBH-1 at 1060.00 m depth representative of S_{1-2} segregated bandings within quartzofeldspathic gneiss. **(b)** Core sample from KBH-5 at 857.40 m depth showing segregated layerings, which are mainly S_{1-2} fabrics. A near-vertical fault surface displacing S_{1-2} fabrics along which secondary precipitations are found. **(c)** Core sample is from KBH-6 at 805.75 m depth exhibiting the same S_{1-2} fabrics within granite gneiss. Interconnected fractures mostly follow the S_{1-2} fabrics orientation. These fractures are filled up with secondary siliceous precipitations. **(d)** Core sample from KBH-7 at 1346.25 m depth representing interlayerings of granite and quartzofeldspathic gneisses with prominent S_{1-2} fabrics. **(e)** Core sample showing sharp contact between Deccan basalt and the underlying granite at 932.5 m depth in borehole KBH-1. Plagioclase laths are prominent within Deccan basalt in the upper portion, while clasts of quartzofeldspathic aggregates are entrapped within the weathered surficial part of granite in the lower part of the sample. **(f)** Core sample collected from 936 m depth in borehole KBH-1 showing anastomosing fractures and ferruginous secondary precipitations. **(g)** Core sample collected from 1159 m depth in borehole KBH-1 showing a fault surface containing downdip slickenlines on a slickenside. **(h)** Core sample showing the sharp contact between Deccan basalt and underlying granitic basement rock at 499.70 m depth in borehole KBH-5. Plagioclase laths are present within Deccan basalt in the upper part of the sample, whereas large quartzofeldspathic clasts entrapped within fine matrix are present in the lower part. **(i)** Core sample from 500.50 m depth in borehole KBH-5 showing prominent downdip slickenlines on a well-developed vertical fault surface. **(j)** Core sample of sheared granite-gneiss from 500.85 m depth in borehole KBH-5, showing lensoid clasts of host rock entrapped within fine-grained gouge matrix of same material within a fractured zone. **(k)** Core sample from 732.00 m depth in borehole KBH-5 showing a near-vertical master fault with associated tensile fractures. A narrow fault zone with brecciated angular fragments of host rock is seen. Angular clasts of host rock are entrapped within fine-grained gouge matrix. The dark black portions along these fractures represent extremely fine grained, pseudotachylite melts injected from the master fault into the associated tensile fractures. **(l)** Core sample showing the sharp contact between Deccan basalt and the underlying granitic basement rock at 775.04 m depth in borehole KBH-6. The basement rock below this contact is highly fractured and shattered. **(m)** Core sample from 897.60 m depth in borehole KBH-6 showing a thin layer of pseudotachylite along the fault surface. Downdip slickenlines are prominently seen on this fault surface. **(n)** Core sample of a fault surface at 948.50 m depth in borehole KBH-6 showing a slickenside with prominently developed slickenlines that formed due to friction during movement. **(o)** Core sample showing highly fractured and brecciated granite rock at 1044.75 m depth in borehole KBH-6. Fragmented clasts of host rock are entrapped within fine matrix of gouge material. Anastomosing fracture network filled with greenish silicification from chanellized water is also observed. **(p)** Core sample showing the direct contact of Deccan basalt and the underlying granitic basement rock at 1251.23 m depth in borehole KBH-7. Plagioclase laths are seen in the first basaltic flow. **(q)** Core sample from 1253.72 m depth in borehole KBH-7 showing fractured quartzofeldspathic layers within granite gneiss. Fractures are filled up with ferruginous precipitations. The mafic layers are mostly weathered and altered in this section. **(r)** Core sample from 1476.70 m depth in borehole KBH-7 showing a mafic dyke (amphibolite) body in a near-vertical orientation and having direct contact with the basement rock.
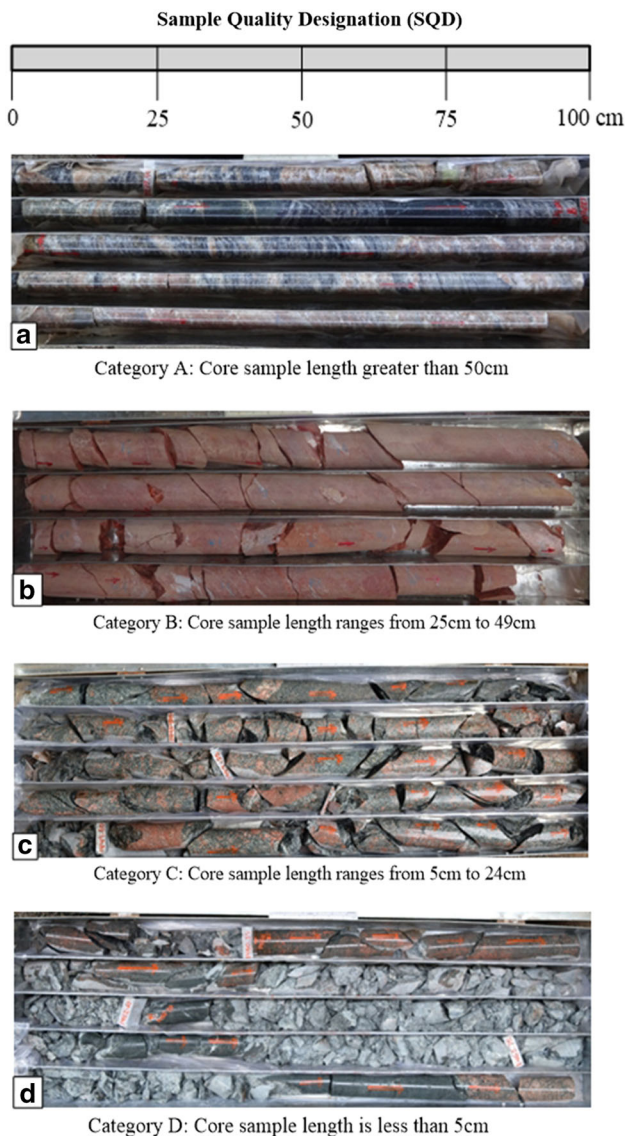
Figure 4. Classification of core samples of basement granitoids by sample quality designation (SQD), an index of deformation based on sample length. **(a)** Cylindrical cores from KBH-7 showing interlayerings of granite, granite gneiss and migmatitic gneiss with SQD category A. **(b)** Core samples from KBH-5 representing sheared granite gneiss with SQD category B. **(c)** Core samples from KBH-6 demonstrating fractured granite and granite gneiss with SQD category C. **(d)** Core samples of KBH-6 representing highly fractured, brecciated and shattered granite and granite gneiss with SQD category D. Physical studies on cores indicate the SQD of categories C and D are from highly fractured and fault zone related rocks at different depths.

basis of associated mineralogy and microstructures, as discussed below.

4.1 *Mineralogy and microstructures of D_1*

Alternate segregated layerings of felsic and mafic minerals are identified on mesoscopic to microscopic scales. Felsic components are dominantly composed of quartz, plagioclase and orthoclase feldspars (majority are microcline), whereas the mafic components are mostly composed of hornblende, biotite, clinopyroxene, occasionally muscovite and intermittently garnet (figure 5a–c). Gneissosity is strongly defined by alternate bandings of quartz + plagioclase feldspar + orthoclase feldspar, and clinopyroxene + hornblende + biotite rich minerals. These are represented as alternate layerings and are labelled in figure 5(a–f), as S_1. Annealed mosaic textures of quartz and feldspar indicate static recrystallization (Passchier and Trouw 2005). Unstrained feldspars and low strained quartz are present following the S_1 (figure 5a). Here, S_1 has been identified as the first developed structural fabric due to preferred alignment of metamorphic minerals. No pre-existing data is available to correlate with the metamorphic event. The first fabrics (S_1) were overprinted and transposed by the later high strain S_2 fabrics (figure 5d–f).

4.2 *Mineralogy and microstructures of D_2*

The D_2 represents strong shearing event and the related planar fabric is termed as S_2. Chlorite, epidote and recrystallized muscovite are aligned along this fabric. Microstructures of quartz show bulging and sub-grain formation within and along grain margins, indicating dynamic recrystallization during this deformation (Passchier and Trouw 2005). Significantly, quartz and feldspar represent variable deformation signatures. In most cases, quartz grains are dynamically recrystallized to form serrated grain boundaries and fine-grained groundmass. Occasionally, feldspars are present as 'augen' shaped clasts surrounded by fine quartz groundmass and form core-mantle structure (Passchier and Trouw 2005). Basement granitoids in KBH-5 are intensely sheared and at places form schists and mylonites. Schistosity within granitoids generally forms due to preferred alignment of micaceous minerals which were developed during metamorphic reactions. Occurrences of kinked geometry within recrystallized muscovite and stabilized chlorite following S_2 fabrics are strongly sheared during this event (figure 5d, e). The shearing is responsible for strong alignment of stretched, boudinaged, quartz ribbons following the S_2 (figure 5f). Structurally the S_2 transposes all pre-existing fabrics (i.e., S_1) following the identical or acute angular orientation.

The textural differences between these two different sets of fabrics indicate a deformation gap in between S_1 and S_2. Therefore, two separate events of deformations, D_1 and D_2, are inferred.

4.3 *Mineralogy and microstructures of D_3*

Significant evidences of brittle deformation such as fault breccia, fault gouge, anastomosing fracture network, pulverized rocks, secondary precipitations along tensile fractures, pseudotachylites and slickenlines on slickensides are observed in the basement granitiods of the seismogenic zone (figure 3e–r). Fault breccias show angular clasts of parent rocks, which are embedded within fine-grained gouge matrix (figure 5i, k). Sets of fractures are present within fault zone rocks at several depths (figure 5h, k). Narrow band of fault gouge material is observed in zones of intense shearing (figure 5g, j, k). The presence of fault breccias and pseudotachylite veins are the direct manifestations of brittle deformation (Sibson 1986; Lin 1996, 2008; Janssen *et al.* 2010). Fault rocks occur with friable gouge material within which clasts of quartzofeldspathic minerals are embedded (figure 3j, k, o, q). Incidences of slickenlines with slickensides are the direct indication of frictional sliding along adjoining fault surfaces (Sibson 1975; Lin 2008). Most of these slickensides are unaltered and show shining lustre within fault zone rocks (figure 3g, i, m, n). Reddish iron staining or ferruginous precipitations are commonly found within anostomosing fractured network (figure 3f, j, o, q). In most cases, e.g., figure 5(l), occurrences of dark black coloured, fine-grained, compact material with tapering ends are present as injected veins from the master fault (figure 3k). These are pseudotachylites that were likely formed due to frictional heating along adjoining master faults during previous earthquakes and may contain a wealth of information about the fault dynamics and earthquake processes (Lin 2008, 2011). All these evidences of brittle deformation are overprinted on the pre-existing textural and structural features S_1 and S_2. Therefore, a separate deformation event D_3 has been identified. A detailed account of these features is presented in the subsequent sections.

5. SEM and EDS studies on fault zone rocks

Detailed studies on fault zone rocks have been performed using Focused Ion Beam – Scanning Electron Microscope (FIB-SEM) and Energy Dispersive X-ray fluorescence system (EDS). Fault breccia (figure 5i) and a pseudotachylite vein (figure 5l) observed in the granitic rocks were selected for detailed analysis to study the textural and elemental composition of fault zone materials.

The Back Scattered Electron (BSE) images obtained from SEM are shown in figure 6(a–f). Spectra were focused on selected points of fault breccia and the pseudotachylite vein, which are shown in electron images in figure 6(e, f). Fault breccia shows angular fragments of parent rock entrapped within a siliceous and ferruginous matrix (figures 5i, j, k, 6a). The host cataclasite is transected by a narrow brecciated zone rich in ferruginous matrix (figure 6b). Both the cataclasite and the narrow brecciated zone are transected by transgranular fractures. The fault breccia is characterized by dense anastomosing fracture network with ferruginous precipitation. The BSE image of figure 6(c) corresponds to the photomicrograph of figure 5(l), which represents a pseudotachylite vein at a depth of 732.55 m in borehole KBH-5. Glassy texture of this pseudotachylite vein material is shown in figure 6(d), revealing both the amorphous and fibrous textures. Amorphous/fibrous textures of pseudotachylites are identified by both the polarized and electron microscopes. These findings may be significant in further detailed studies to characterize seismic slip (Lin 2008; Lin *et al.* 2015; Lin and Nishiwaki 2019).

The BSE images of the fault breccia and pseudotachylite vein are shown in figure 6(e and f). Spectra were focused at several points on these two images and analysed by using X-ray diffraction in FIB-SEM. Detailed elemental percentage at these points are presented in tables 2 and 3. The dataset represents a significant difference in the composition between clasts and matrix within the fault breccia, especially in the fault gouge material. The elemental studies on fault breccias also reveal compositional differences between host rock and secondary precipitations. Angular fragmented clasts of quartzofeldspathic aggregates are entrapped in the fine-grained matrix. Fine-grained matrices are formed by chemical alterations and secondary precipitations within the fault zone. Fragmented clasts present within fault zone materials (fault breccias and gouge) have different elemental wt.% when compared with the matrix (table 2). Secondary precipitations present in the fractures of fault breccia are also shown in terms of elemental wt.%. The clasts have wt.% ranges of O: 44.58–53.09, Al: 0.05–10.51, Si: 30.42–46.46, Ca:
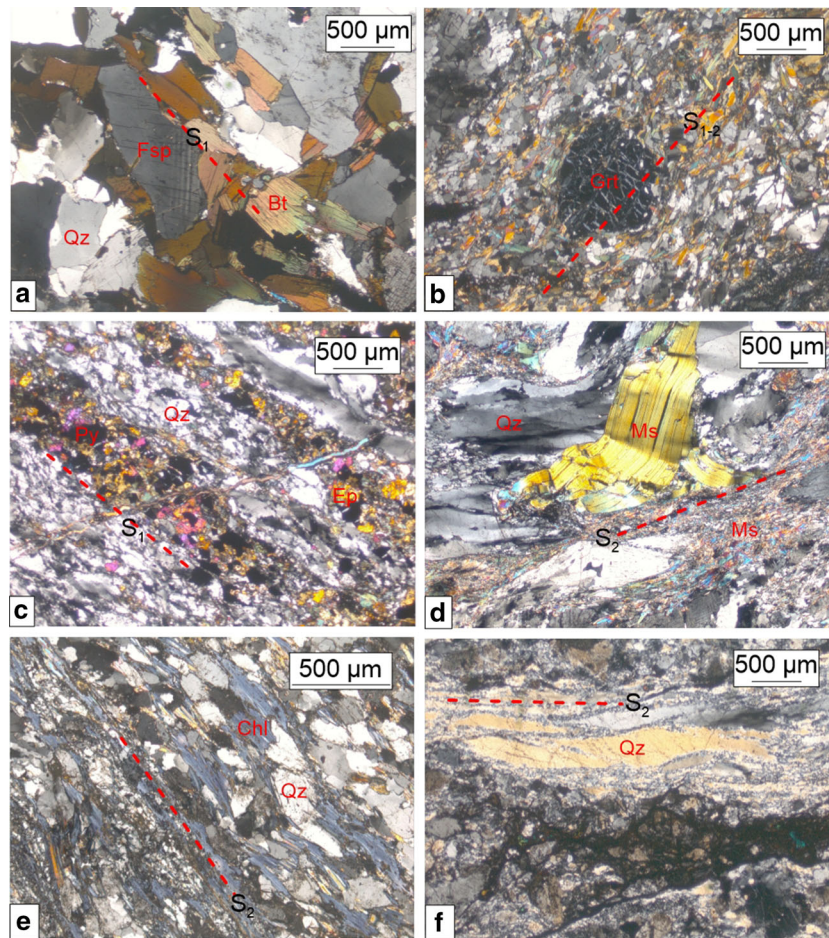
Figure 5. Photomicrographs of basement granitoids representing mineralogy and deformation signatures of both ductile and brittle events in the Koyna seismogenic zone. (a) Granite gneiss showing biotite (Bt) defined gneissosity (S_1) under microscope. (b) Garnet (Grt)–biotite (Bt)–muscovite (Ms) defined fabric within granite-gneiss representing both S_1 and S_2. (c) Alternate layerings of recrystallized quartz (Qz)–feldspars (Fsp) rich felsic and pyroxene (Py)–biotite (Bt)–epidote (Ep) rich mafic layers representing gneissosity of S_1 within granite gneiss. (d) High D_2 strained rock showing kinked and recrystallized muscovite (Ms) along the S_2 fabric. (e) Chlorite defined fabric within granite schist indicating S_2 fabric that formed with dynamically recrystallised quartz grains. (f) Quartz (Qz) ribbon within high D_2 strained rock surrounded by dynamically recrystallised quartz grains. The lower dark portion indicates fracture network that is overprinted on D_2 structures and these fractures are filled up with ferruginous material. (g) Cataclasite of granite rock where clasts of quartzofeldspathic aggregates are embedded within fine-grained quartz-rich matrix. (h) Narrow fault zone within granite, which developed during D_3 event. This fractured zone is filled up with gouge material. (i) Fault breccia observed within granite wherein angular fragments of quartz and plagioclase feldspars (Pl) are embedded within matrix of gouge and siliceous precipitations. (j) Set of trans-granular fractures (Fr) developed during D_3 deformation. (k) Narrow band of fault gouge transecting coarse-grained granite following a micro-fault zone. (l) Photomicrograph of a pseudotachylite vein that intruded along a tensile fracture within the basement of granite gneiss at 732.50 m depth in borehole KBH-5.

0.04–0.61, Fe: 0.19–0.34, Na: 0.00–9.07, and K: 0.00–12.84. In contrast, the fine-grained matrix has different elemental wt.% ranges of O: 44.42–45.20, Al: 12.36–13.65, Si: 17.85–18.26, Ca: 15.12–15.46, Fe: 7.74–9.58, Na: 0.00–0.11, and K: 0.00–0.33. Hence, the matrix is rich in Ca and Fe when compared with the fragmented clasts. Enrichment of these elements within fine-grained matrix groundmass could be related with secondary mineralization and ferruginous precipitations along

fractures in the brecciated rocks (Lin 2008; Lin *et al.* 2015; Moore and Lockner 2013; Lin and Nishiwaki 2019).

Compositional and textural studies on pseudotachylites can provide significant information about earthquakes and are therefore often known as 'earthquake fossils' (Lin 2008). Physically, pseudotachylite veins are dark black in colour with fine-grained appearances along the fault surfaces (figure 3k, m). These veins are associated with fault
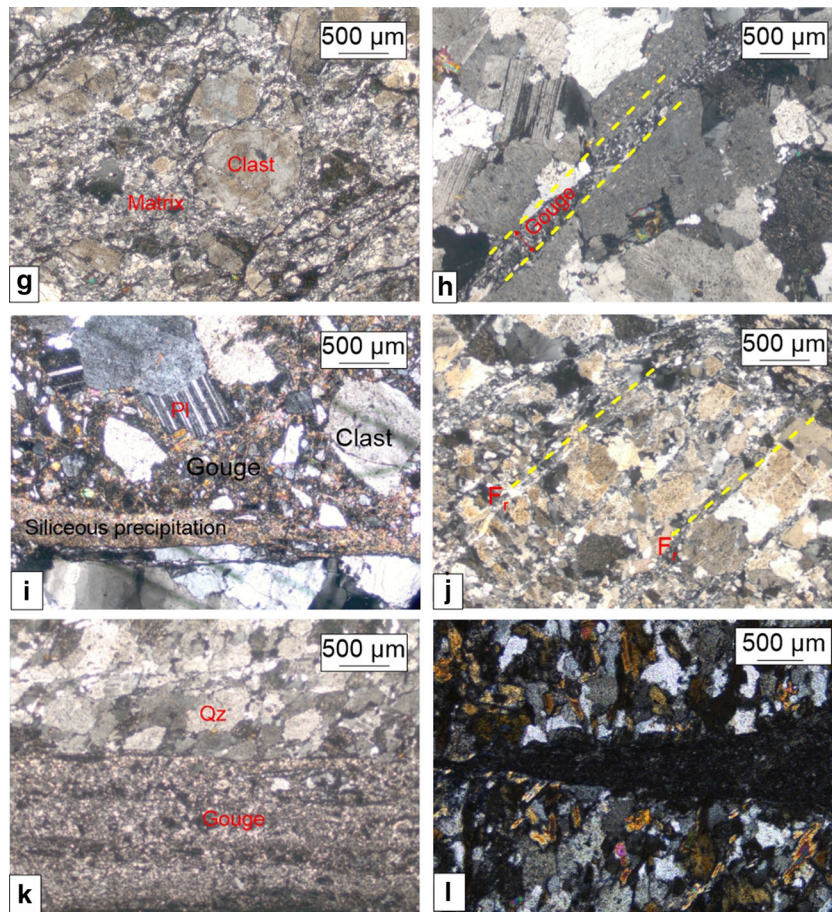
Figure 5. (*Continued.*)

breccias and fault gouge, prominent slickenlines on slickensides and show shining lustre. Elemental wt.% of the pseudotachylite vein is represented by O: 45.58–49.54, Na: 0.00–0.44, Mg: 0.35–14.34, Al: 8.37–10.37, Si: 16.24–30.48, K: 0.04–12.47, Ca: 0.00–0.42, and Fe: 0.37–13.26. The wt.% of Fe and Ca represent the composition of unaltered pseudotachylite material; no secondary precipitation or alteration are observed within this vein. The wt.% of Al, Si and O are higher than other elements, and the wt.% of Fe, Mg and K show a wide range (table 3). Pseudotachylites are commonly formed due to sudden cooling of a melt. The melt is generally produced because of frictional heating along faults during earthquakes (Sibson 1973, 1975; Rice 2006; Lin 2008). As a result, composition of pseudotachylites are directly dependant on the mineralogy of the host rocks adjacent to faults (Lin 2008; Jiang *et al.* 2015). Here, pseudotachylites show amorphous and fibrous textures (figure 6d), and characterized by glassy material that is rich in Si and O, while the presence of Al, Fe, Mg and K indicate presence of feldspars and other mafic contents within the host granites and gneisses.

6. Discussion

Scientific deep drilling in the Koyna seismogenic zone provides a rare opportunity to sample and study the granitic basement rock below the Deccan Traps. The recurrent seismic activity in the region over the past 55 years is concentrated within the granitic basement rocks buried under a kilometer thickness of flood basalts and extends to a depth of ~ 10 km from the surface (Gupta *et al.* 2015). The core samples of basement granitoids down to 1.5 km depth, recovered from boreholes drilled in close proximity to the epicentral region, therefore, make a good case to study the deformation signatures in general and co-seismic deformation and related structural features in particular. Petrography and microstructural studies carried out in the present study show that structural features and deformation signatures observed in the cores of basement granitoids preserve significant information about brittle deformation.

Basement core specimens from boreholes, KBH-1, KBH-5, KBH-6 and KBH-7 provide compelling evidences to infer the sequence of deformation in
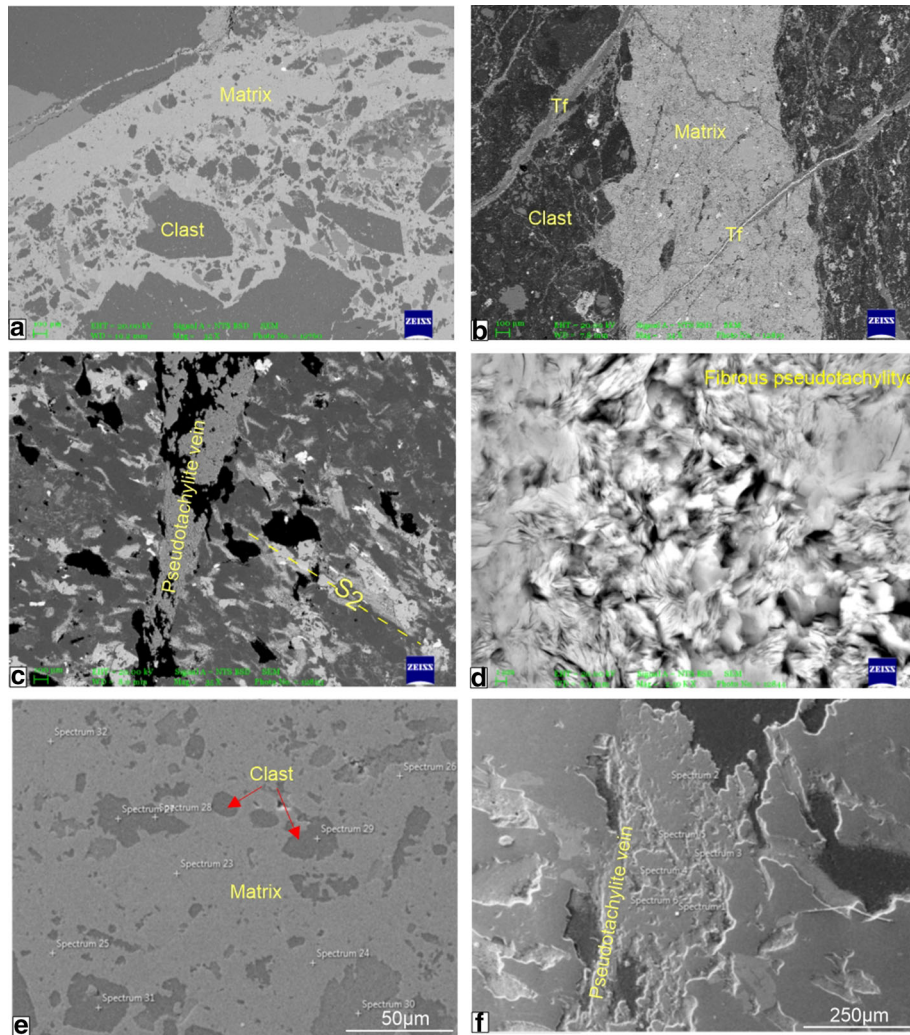
Figure 6. SEM-BSE images of fault rocks and pseudotachylite veins sampled from basement granites and EDS analyses to characterize the fault zone materials. **(a)** SEM-BSE image of a fault breccia representing a domain similar to figure 5(i). Angular fragments of quartzofeldspathic material are entrapped within fine siliceous and ferrugenious matrix. The section represents 1354.15 m depth in borehole KBH-7. **(b)** SEM-BSE image of a fault zone rock at 511.04 m depth in KBH-5, representing repeated brittle fracturing of rocks along which siliceous and ferruginous precipitations occurred. **(c)** SEM-BSE image of a pseudotachylite vein (representing a domain similar to figure 5l), sharply transecting the gneissosity of the country rock at a high angle at 732.50 m depth in KBH-5. **(d)** SEM-BSE image of the same pseudotachylite vein under very high magnification, revealing fibrous nature of the pseudotachylite material that formed due to sudden cooling of melt produced during seismic activity. **(e)** Electron image of fault rock collected from the similar domain of figure 6(a) showing locations of spectra 23–32 at which EDS analysis has been done. Dark coloured areas represent the clasts and light coloured areas represent cemented gouge/matrix. The data are given in table 2. **(f)** Electron image of the same pseudotachylite vein as shown in figure 6(c). Locations of spectra 1–6, at which EDS analysis has been done, are shown and the data are given in table 3.

the region. The basement rock is a complex of granite, granite-gneiss and migmatitic gneiss. Strongly developed segregation bandings are observed within the gneissic domains. The mineral assemblage of pyroxene + hornblende + biotite $\pm$ garnet $\pm$ muscovite following the S_1 fabric indicates amphibolite facies condition, which prevailed during D_1 event, whereas the assemblage chlorite + epidote + recrystallized muscovite and dynamically recrystallized quartz minerals within the S_2 fabric suggest that greenschist facies prevailed during D_2 event. The occurrence of mylonites, S-C fabrics within muscovite-rich granite-schists, recrystallized quartz-rich groundmass, serrated quartz grain boundaries indicate high strain condition during D_2 deformation. The pre-existing D_1 and D_2 features are overprinted by cataclasite, fault breccias and fault gouge. These latter brittle deformation features are identified as D_3 event. The information available so far is inadequate to

determine whether the D₃ deformation event could be the manifestation of the recurrent seismicity over the past 55 years in the area. Association of pseudotachylites with slickenlines on slickensides preserved within the fault zones support frictional deformation. Cores recovered from all the four boreholes show clear evidences of faulting, fracturing and superposition of breccias with transgranular fractures and fault gouge, which are indicative of multiple episodes of brittle deformation. Cataclasites with multiple deformations are also found locally away from the fault zones. Frequent occurrences of microcracks, fault-breccias and cataclasites in drill core samples confirm that the faults were reactivated in a brittle regime (Ismat and Mitra 2001; Passchier and Trouw 2005; Matin and Misra 2009).

Basement rocks record evidence of intensive fractures and fissures which were developed during D₃ deformation. In the majority of the boreholes, fractures generally follow the pre-existing weak planes such as foliations although other orientations are also observed. The fault and fracture zones (SQD category C and D) are dominantly characterized by intense shattering and brecciation. Occurences of slickenlines with slickensides and pseudotachylites are mostly associated with intense shattering and brecciation. Well-developed fractures in the basement granitoids show prominent striations with shining lustre on the slickensides (figure 3g, i, j, m, n). Very little or no geochemical alterations are observed on such fault and fracture surfaces. In fact, most of these faults and fractures are filled up with secondary precipitation, which provide evidences for the presence of water at depth.

In this study, the angles of fractures and foliations measured with respect to the vertical borehole axis are plotted in figure 7. Fractures and foliations in the KBH-1 and KBH-5 borehole cores show nearly identical orientations (figure 7a–d). In case of borehole KBH-6, only a few fractures follow the foliation, whereas most of the fractures have different angles which are near vertical (figure 7e, f). Intensive shattering and brecciation of cores in borehole KBH-6 are directly related with near-vertical faults/fractures. Notably, pseudotachylite veins are also associated with these sub-vertical faults and fractures (figure 3k, m, n). Additionally, these near-vertical faults and fractures are largely unaltered, containing lustrous slickensides with prominent downdip slickenlines. In borehole KBH-7, fracture angles show a wide range of 0°–90°.
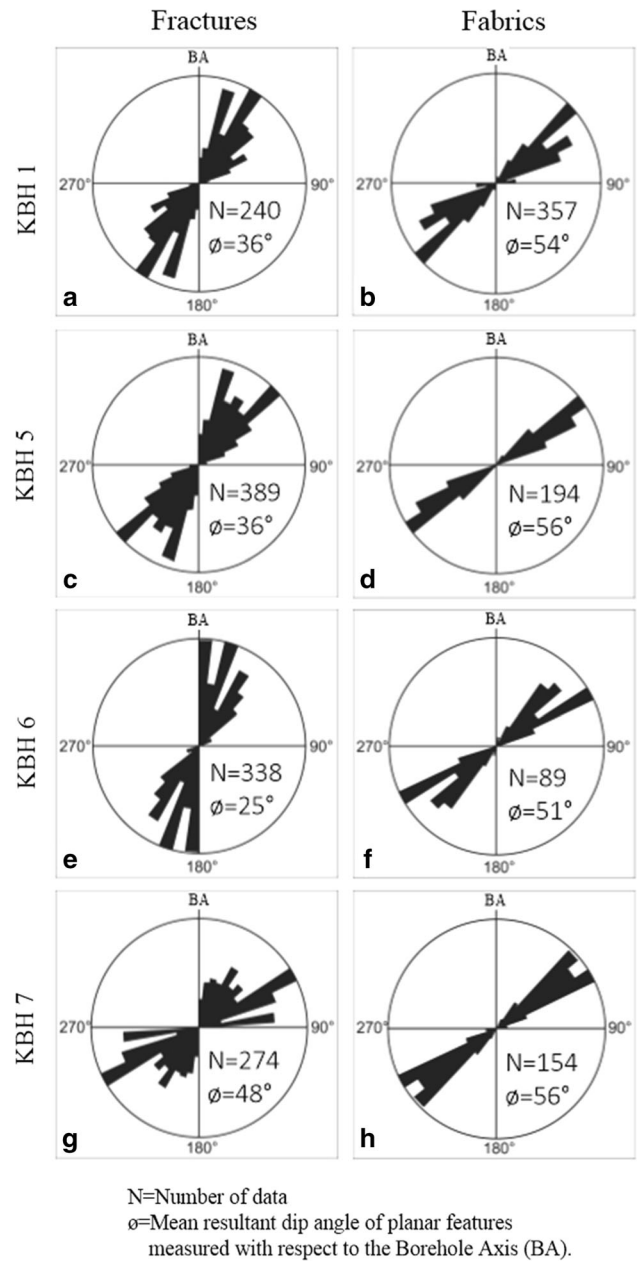

Figure 7. Rose diagrams representing the distribution of angles of foliations (N=794) and fractures (N=1241) measured with respect to the vertical borehole axis (BA) in KBH-1, KBH-5, KBH-6 and KBH-7. Note that in most cases, natural fractures and fabrics show similar range of orientations except in borehole KBH-6 in which near-vertical fractures dominate. These near-vertical fractures likely formed due to faulting of rocks in close association with a near-vertical fault.

Here, they have identical orientations with the foliations, however, there are other orientations which represent localized faulting and fracturing activities (figure 7g, h). Importantly, the borehole KBH-7 is located in the proximity of the NNE–SSW trending and steeply dipping Donichawadi fault zone. The wide range of fracture angles in borehole KBH-7 may be associated with the

vertical movements in the Donichawadi fault zone. Filling of fractures and fissures with secondary precipitations suggests fluid-filled tensile fractures and fissures which are closely associated with this near-vertical fault zone. Occurences of prominent downdip slickenlines on shining slickensides with thin layers of pseudutachylites are the strong evidences of frictional shearing which are mostly unaltered. In conclusion, it can be inferred that the D_3 deformation zone present within the basement rocks is an ongoing process of vertical movement within an extensional fault zone. The frictioned surfaces preserve the evidences of elastico-frictional deformation, and, tensile openings are filled up with secondary precipitations within the same fault zone.

A recent study by Goswami *et al.* (2020) has determined fracture dip amounts and orientations from borehole image logs acquired in a 3014-m deep research borehole, called the Koyna Pilot Borehole KFD1 drilled within the Koyna seismogenic zone (figure 1). Downhole geophysical measurements confirmed that the borehole KFD1 had penetrated fault damage zones at multiple depth intervals in the granitic basement below 2100 m (Goswami *et al.* 2019). The borehole KFD1, located in the proximity of the exploratory borehole KBH-7, passed through 1247 m thick Deccan Trap and continued ∼1767 m into the underlying granitic basement rocks (Roy 2017). The borehole images were oriented with respect to the true north and as many as 2226 shear fractures were picked manually in the 1767 m long basement section. The dip amount of the fractures shows a wide range from sub-horizontal ($\leq 10°$) to subvertical ($\geq 80°$) and the majority of the fracture strike azimuths show a range from NNE to NNW (figure 8)
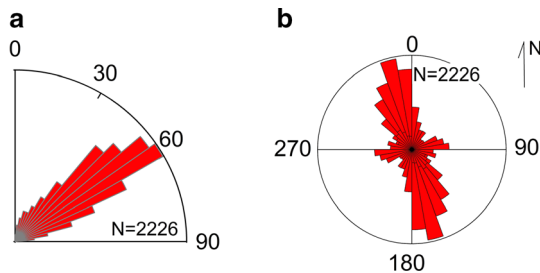

Figure 8. Rose diagrams showing the distributions of dip amounts and strike azimuths of shear fractures identified from borehole images in the 1767 m long granitic basement section in Koyna Pilot Borehole KFD1. The borehole images are oriented with respect to the true north and 2226 shear fractures between 1247 and 3014 m depth are studied.

Table 2. *EDS analysis of a fault breccia recovered from KBH-7 basement granite rock showing wt.% of elements. The spectrum points shown in electron image of figure 6(e) are studied under FIB-SEM.*

Element	Spectrum 23 (Gouge)	Spectrum 24 (Gouge)	Spectrum 25 (Gouge)	Spectrum 26 (Gouge)	Spectrum 27 (Clast)	Spectrum 28 (Clast)	Spectrum 29 (Clast)	Spectrum 30 (Clast)	Spectrum 31 (Clast)	Spectrum 32 (Gouge)
O	44.42	44.93	45.20	44.83	53.09	52.96	48.30	44.58	48.00	44.77
Na	00.01	00.00	00.01	00.02	00.00	00.00	08.42	00.29	09.07	00.11
Mg	00.00	00.01	00.09	00.04	00.07	00.01	00.00	00.00	00.00	00.00
Al	12.36	13.65	13.24	12.88	00.05	00.06	08.99	10.25	10.51	12.69
Si	18.26	18.09	17.95	17.96	46.36	46.46	32.93	30.42	32.11	17.85
S	00.00	00.01	00.01	00.00	00.02	00.00	00.03	00.00	00.00	00.00
K	00.05	00.00	00.33	00.03	00.00	00.01	00.03	12.84	00.04	00.02
Ca	15.31	15.46	15.12	15.36	00.14	00.13	00.61	00.04	00.05	15.45
Mn	00.01	00.12	00.18	00.03	00.00	00.16	00.07	00.00	00.00	00.09
Fe	09.58	07.74	07.86	08.35	00.24	00.20	00.34	00.19	00.20	09.01
Th	00.01	00.00	00.00	00.02	00.03	00.00	00.29	00.11	00.00	00.00
Total	100.00	100.00	99.99	99.52	100.00	99.99	100.00	98.72	99.98	99.90

Table 3. *EDS analysis on a pseudotachylite vein recovered from KBH-5 basement granite-gneiss showing wt.% of elements. The spectrum points shown in electron image of figure 6(f) were studied under FIB-SEM.*

Element	Spectrum 1	Spectrum 2	Spectrum 3	Spectrum 4	Spectrum 5	Spectrum 6
O	45.74	48.20	48.06	49.54	45.58	45.90
Na	00.22	00.18	00.00	00.44	00.06	00.01
Mg	01.38	01.17	14.34	13.95	14.16	00.35
Al	10.11	09.81	08.91	08.37	09.43	10.37
Si	29.41	28.06	16.36	16.24	16.85	30.48
P	00.00	00.00	00.01	00.06	00.02	00.00
K	11.79	11.93	00.04	00.04	00.21	12.47
Ca	00.00	00.09	00.23	00.11	00.42	00.02
Fe	01.35	00.55	11.43	10.72	13.26	00.37
Th	00.00	00.00	00.17	00.00	00.00	00.00
Total	100.00	99.99	99.55	99.47	99.99	99.97

(Goswami *et al.* 2020). Significantly, the trend of the fractures obtained from borehole images is consistent with the surface fissures mapped in the Donichawadi fissure zone by GSI (1968) and in the surrounding areas by Misra *et al.* (2017). The study carried out by Goswami *et al.* (2020) provided a sound basis for correlating subsurface data from basement granitoids with the surface manifestations in the Koyna region.

A structural correlation can be established between the boreholes KFD-1 and KBH-7 taking advantage of their proximity. The basalt thickness in the two boreholes are quite similar, 1247 m and 1251 m, respectively. Study of KBH-7 core samples shows that majority of the fractures dip in the range 30°–80° with a mean of 48° (figure 7g). Thus, dip amounts of the inclined fractures observed in borehole KFD1 are consistent with the fracture angles measured in the KBH-7 basement core. However, the unoriented KBH-7 cores do not allow determination of strike azimuths. Since the boreholes KFD1 and KBH-7 are located close to each other and the dip amounts of the fractures are also consistent; therefore we can infer that the subsurface fracture strike azimuths at the KBH-7 site may be similar to those at the KFD1 borehole site. Additionally, both the boreholes are located in the vicinity of the Donichawadi fissure zone, which is a surface manifestation of the 1967 *M* 6.3 Koyna earthquake. The en-echelon fractures, oblique or diagonal tensile cracks and mole cracks associated with the Donichawadi fissure zone are oriented in the range N10ºW to N25ºE, which are very consistent with the strike azimuths of the shear fractures observed in the borehole KFD1. A study

of structural orientations of these fissures shows that the principal orientation of the fissure zone is 25°/89°-E (Misra *et al.* 2017). A soil-gas helium study across the Donichawadi fissure zone (Gupta *et al.* 1999) and later online gas monitoring study during the drilling of the Koyna pilot borehole KFD1 (Podugu *et al.* 2019) have shown similar high levels of helium concentration (up to 12.8 ppmv), which confirm that the fissure is the surface manifestation of a subsurface fault/fracture zone and that the fault zone has not healed during the past 50 years. The consistency of the strike azimuths of the subsurface fault(s)/fractures with the surface fissures and the conductive nature of fault zone suggest that the interconnected fractures provide pathways for fluids to enter the fault zone(s). This could trigger earthquakes either by increasing fluid pressure in the fault zone or by decreasing the frictional strength of the fault gouge in the region.

During earthquake occurrence, up to 90% of the released energy is used to overcome the frictional strength of the fault (Kanamori and Brodsky 2004; Scholz 2002 and references therein; Rice 2006). Friction generates high temperature at the interface between the two sliding blocks causing the rock to melt and get injected into the fractures/ veins adjacent to the principal slip zone. Cooling of such melts form pseudotachylites, which therefore provides information about seismic activity and energy budget of the earthquake (Sibson 1975, 1986; Lin 1996, 2008, 2011; Cowan 1999; Nielsen *et al.* 2008; Beeler *et al.* 2016; Aubry *et al.* 2018). In the present study, pseudotachylites are observed at multiple depths along veins/fractures. The FIB-SEM and EDS analyses carried out on

fault rocks and pseudotachylites yield significantly different elemental composition. The clasts present in the brecciated section of the fault zone are mostly quartz and feldspars embedded within a fine-grained matrix. Compositional analysis of clasts, matrix and pseudotachylites show substantial differences in wt.% of Fe, Ca and Al between host rock and the secondary products. Higher percentage of Fe, Ca and Al are observed within the matrix when compared with the host rock. On the other hand, secondary products are mostly formed by siliceous and ferruginous precipitations in a fault zone (Sibson 1975, 1986; Lin 2008, 2011; Warr *et al.* 2014; Lin and Nishiwaki 2019). Presence of calcite crystals and sericitized feldspars along fractures are responsible for high wt.% of Ca and Al within the fault zone (table 2). The EDS studies on pseudotachylite veins show a large variation of elemental wt.% for Fe, Mg and K, whereas the wt.% of Al remains high throughout the domain, pointing to its source from feldspar rich country rock adjacent to the pseudotachylite veins. Amorphous/fibrous textures and compositional variations of pseudotachylites are related with the mechanism of shearing during friction (Lin 2008, 2011; Warr *et al.* 2014; Lin and Nishiwaki 2019). This compositional variation is similar to the mineralogy of the host rock. Amorphous/fibrous textures and compositional variations of pseudotachylites are related to the total increase in temperature during friction (Lin 2008, 2011; Warr *et al.* 2014; Lin and Nishiwaki 2019). Age dating of the pseudotachylites could shed more light on their possible association with seismic activity in the region.

7. Conclusions

(1) The basement rock in the Koyna seismogenic zone comprises granite and granite-gneiss inter-layered with variable proportions of migmatitic gneiss, typically representative of the Peninsular Gneiss of the Dharwar Craton in south India. The metamorphic mineral assemblages of these basement granitoids indicate amphibolite to greenschist facies metamorphism.

(2) The basement rocks record three successive deformation events, D_1, D_2 and D_3. While D_1 and D_2 are associated with ductile deformation, D_3 is associated with brittle or frictional deformation and could be a result of past seismic activity in the region.

(3) The study on drill cores down to 1.5 km depth in the area has brought out the relationship between the fractures and the foliation in the fault zone rocks, suggesting variable angular relation both within a borehole column as well as between different boreholes. Fractures do not necessarily follow pre-existing weak planes during their development. Also, fault brecciation and shattering of rocks are observed along near-vertical fractures. Vertical fractures differ significantly from the mean angle of foliations observed in the basement granitoids, which indicates that local stress kinematics play a major role in their development.

(4) Presence of prominent dip-slip slickenlines on near-vertical slickensides indicates vertical movement of a fault along its surface(s). Most of these fractures are tensile in nature, which implies an extensional faulting mechanism at depth.

(5) Occurrences of fault breccia and fault gouge along with pseudotachylites, slickenlines and slickensides indicate frictional deformation within the fault zone(s). The presence of different sets of fractures and their dispositions point to multiple episodes of brittle deformations within the fault zone(s). Most of these fractures are filled with ferruginous and/or siliceous precipitation that indicate the presence of water at depth.

(6) FIB-SEM and EDS studies on fault gouge and pseudotachylite veins confirm secondary precipitation following the anastomosing fracture networks. The secondary minerals are unusually rich in Fe and Ca, consistent with the host rock. Composition of pseudotachylite shows higher wt.% of O, Al and Si than the composition of parent rock-forming minerals, although at places, pseudotachylite has higher Fe, Mg and K content.

Author statement

Surajit Misra was involved as 'Project Scientist C' under the Scientific Deep Drilling programme since 2014–2017. He is fully involved with rigorous geological data collection, thin sections preparation for polarizing microscope and SEM-EDS analyses, analysis of structural data from mesoscopic to microscopic scale, analysis of geochemical data, conceptualization of the problem, collection of background information, initial writing of the manuscript, preparation of images with complete figures, discussions with co-authors and finalization of the manuscript up to submission. Deepjyoti Goswami was involved in borehole geophysical data acquisitions, its processing and interpretations. Sukanta Roy contributed in improving interpretation, technical and grammatical correction, and finalization of the manuscript.

References

Allen M J, Tatham D, Faulkner D R, Mariani E and Boulton C 2017 Permeability and seismic velocity and their anisotropy across the Alpine Fault, New Zealand: An insight from laboratory measurements on core from the Deep Fault Drilling Project phase 1 (DFDP-1); *J. Geophys. Res. Solid Earth* **122** 6160–6179, https://doi.org/10.1002/2017JB014355.

Ando M 2001 Geological and geophysical studies of the Nojima Fault from drilling: An outline of the Nojima Fault Zone Probe; *Island Arc* **10** 206–214, https://doi.org/10.1111/j.1440-1738.2001.00349.x.

Aubry J, Passelègue F X, Deldicque D, Girault F, Marty S, Lahfid A, Bhat H S, Escartin J and Schubnel A 2018 Frictional heating processes and energy budget during laboratory earthquakes; *Geophys. Res. Lett.* **45** 12,274–12,282, https://doi.org/10.1029/2018GL079263.

Barton C A and Zoback M D 1994 Stress perturbations associated with active faults penetrated by boreholes: Possible evidence for near-complete stress drop and a new technique for stress magnitude measurements; *J. Geophys. Res.* **99** 0148–0227, https://doi.org/10.1029/93JB03359.

Beane J E, Turner C A, Hooper P R, Subbarao K V and Walsh J N 1986 Stratigraphy, composition and form of the Deccan basalts, Western Ghats, India; *Bull. Volcanol.* **48** 61–83, https://doi.org/10.1007/BF01073513.

Beeler N M, Di Toro G and Nielsen S 2016 Earthquake source properties from Pseudotachylite; *Bull. Seismol. Soc. Amer.* **106(6)** 2764–2776, https://doi.org/10.1785/0120150344.

Ben-Zion Y and Sammis C G 2003 Characterization of fault zones; *Pure Appl. Geophys.* **160(3)** 677–715, https://doi.org/10.1007/PL00012554.

Bondre N R, Duraiswami R A and Dole G 2004 Morphology and emplacement of flows from the Deccan Volcanic Province, India; *Bull. Volcanol.* **66** 29–45.

Boness N L and Zoback M D 2004 Stress-induced seismic velocity anisotropy and physical properties in the SAFOD Pilot Hole in Parkfield, CA; *Geophys. Res. Lett.* **31** L15S17, https://doi.org/10.1029/2003GL019020.

Boullier A M 2011 Fault-zone geology: Lessons from drilling through the Nojima and Chelungpu faults; *Geol. Soc. London, Spec. Publ.* **359(1)** 17, https://doi.org/10.1144/SP359.2.

Bradbury K K, Barton D C, Solum J G, Draper S D and Evans J P 2007 Mineralogic and textural analyses of drill cuttings from the San Andreas Fault Observatory at Depth (SAFOD) boreholes: Initial interpretations of fault zone composition and constraints on geologic models; *Geosphere* **3(5)** 299–318, https://doi.org/10.1130/GES00076.1.

Bradbury K K, Evans J P, Chester J S, Chester F M and Kirschner D L 2011 Lithology and internal structure of the San Andreas Fault at depth based on characterization of phase 3 whole-rock core in the San Andreas Fault Observatory at Depth (SAFOD) borehole; *Earth Planet. Sci. Lett.* **310** 131–144, https://doi.org/10.1016/j.epsl.2011.07.020.

Bradbury K K, Davis C R and Shervais J W 2015 Composition, alteration, and texture of fault-related rocks from Safod Core and surface outcrop analogs: Evidence for deformation processes and fluid-rock interactions; *Pure Appl. Geophys.* **172** 1053–1078, https://doi.org/10.1007/s00024-014-0896-6.

Brudy M, Zoback, M D, Fuchs, K, Rummel F and Baumgärtner J 1997 Estimation of the complete stress tensor to 8 km depth in the KTB scientific drill holes: Implications for crustal strength; *J. Geophys. Res.* **102 (B8)** 18,453–18,475, https://doi.org/10.1029/96JB02942.

Caine J S, Evans J P and Forster C B 1996 Fault zone architecture and permeability structure; *Geology* **24(11)** 1025–1028.

Carpenter B M, Marone C and Saffer D M 2009 Frictional behaviour of materials in the 3D SAFOD volume; *Geophys. Res. Lett.* **36** L05302, https://doi.org/10.1029/2008GL036660.

Carpenter B M, Saffer D M and Marone C 2012 Frictional properties and sliding stability of the San Andreas fault from deep drill core; *Geology* **40(8)** 759–762, https://doi.org/10.1130/G33007.1.

Carpenter B M, Kitajima H, Sutherland R, Townend J, Toy V G and Saffer D M 2014 Hydraulic and acoustic properties of the active Alpine Fault, New Zealand: Laboratory measurements on DFDP-1 drill core; *Earth Planet. Sci. Lett.* **390** 45–51, https://doi.org/10.1016/j.epsl.2013.12.023.

Courtillot V, Besse J, Vandamme D, Montigny R, Jaeger J J and Cappetta H 1986 Deccan flood basalts at the Cretaceous/Tertiary boundary?; *Earth Planet. Sci. Lett.* **80** 361–374.

Courtillot V, Feraudt G, Maluski H J, Vandamme D, Moreau M G and Besse J 1988 Deccan flood basalts and the Cretaceous/Tertiary boundary; *Nature* **333**.

Cowan D S 1999 Do faults preserve a record of seismic slip? A field geologist's opinion; *J. Struct. Geol.* **21** 995–1001.

Cox K G and Hawkesworth C J 1985 Geochemical stratigraphy of the Deccan Traps at Mahabaleshwar, Western Ghats, India, with implications for open system magmatic processes; *J. Petrol.* **26** 355–377.

Devey C W and Lightfoot P J 1986 Volcanological and tectonic control of stratigraphy and structure in the western Deccan Traps; *Bull. Volcanol.* **48** 195–207.

Duncan R A and Pyle D G 1988 Rapid eruption of Deccan flood basalts, Western India; *Geol. Soc. India Memoir* **10** 1–9.

Evans J P and Chester FM 1995 Fluid-rock interaction in faults of the San Andreas system: Inferences from San Gabriel fault rock geochemistry and microstructures; *J. Geophys. Res.* **100(B7)** 13,007–13,020, https://doi.org/10.1029/94JB02625.

Evans J P, Forster C B and Goddard J V 1997 Permeabilities of fault-related rocks and implications for fault-zone hydraulic structure; *J. Struct. Geol.* **19(11)** 1393–1404.

Faulkner D R and Rutter E H 2003 The effect of temperature, the nature of the pore fluid, and subyield differential stress on the permeability of phyllosilicate-rich fault gouge; *J. Geophys. Res.* **108** 2227, https://doi.org/10.1029/2001JB001581,B5.

Faulkner D R, Mitchell T M, Healy D, Heap M J 2006 Slip on weak faults by the rotation of regional stress in the fracture damage zone; *Nature* **444(7121)** 922–925, https://doi.org/10.1038/nature05353.

Goswami D, Roy S and Akkiraju V V 2019 Delineation of damage zones from 3 km downhole geophysical logs in the Koyna Seismogenic zone, western India; *J. Geophys. Res.-Solid Earth* **124**, https://doi.org/10.1029/2018JB017257.

Goswami D, Hazarika P and Roy S 2020 *In-situ* stress orientation from 3 km borehole image logs in the Koyna Seismogenic Zone, western India: Implications for transitional faulting environment; *Tectonics* **39** e2019TC005647, https://doi.org/10.1029/2019TC005647.

GSI 1968 A Geological Report on the Koyna Earthquake of 11th December 1967, Satara District, Maharashtra state; Report submitted by officers of the GSI, 273p (incl. plates).

Gupta H K 1992 *Reservoir induced earthquakes*; Elsevier Scientific Publishing Company, Amsterdam, 364p.

Gupta H K 2002 A review of artificial reservoir triggered earthquakes with special emphasis on earthquakes in Koyna, India; *Earth Sci. Rev.* **58** 279–310.

Gupta H K 2011 Artificial water reservoir triggered earthquakes; In: *Encyclopaedia of Solid Earth Geophysics* (ed.) Gupta H, Springer, Berlin, pp. 15–24.

Gupta H K 2017 Koyna, India, an ideal site for near field earthquake observations; *J. Geol. Soc. India* **90(6)** 645–652, https://doi.org/10.1007/s12594-017-0771-z.

Gupta H K and Dwivedy K K 1996 Drilling at Latur Eathquake region exposes a peninsular gneiss basement; *J. Geol. Soc. India* **47** 129–131.

Gupta H K, Rao R U M, Srinivasan R, Rao G V, Reddy G K, Dwivedy K K, Banerjee D C, Mohanty R and Satyasaradhi Y R 1999 Anatomy of surface rupture zones of two stable continental region earthquakes, 1967 Koyna and 1993 Latur, India; *Geophys. Res. Lett.* **26(13)** 1985–1988.

Gupta H K, Rao N P, Roy S, Arora K, Tiwari V M, Patro P K, Satyanarayana H V S, Shashidhar D, Mallika K, Akkiraju V V, Goswami D, Vyas D, Ravi G, Srinivas K N S S S, Srihari M, Mishra S, Dubey S, Raju C P, Borah U, Reddy C V, Babu K C, Rohilla S, Dhar U, Sen M K, Bhaskar Rao Y J, Bansal B K and Nayak S 2015 Investigations related to scientific deep drilling to study reservoir-triggered earthquakes at Koyna, India; *Int. J. Earth Sci.* **104** 1511–1522, https://doi.org/10.1007/s00531-014-1128-0.

Gupta H K, Arora K, Rao N P, Roy S, Tiwari V M, Patro P K, Satyanarayana H V S, Shashidhar D, Mahato C, Srinivas K N S S S, Srihari M, Satyavani N, Srinu Y, Gopinadh D, Raza H, Monikuntala J, Akkiraju V V, Goswami D, Vyas D, Dubey C P, Raju D, Borah U, Raju K, Chinnareddy K, Babu N, Bansal B K and Nayak S 2016 Investigations of continued reservoir triggered seismicity at Koyna, India; *Geol. Soc. London, Spec. Publ.* **445**, https://doi.org/10.1144/SP445.11.

Hickman S and Zoback M 2004 Stress orientations and magnitudes in the SAFOD pilot hole; *Geophys. Res. Lett.* **31** L15S12, https://doi.org/10.1029/2004GL020043.

Holdsworth R E, van Diggelen E W E, Spiers C J, de Bresser J H P, Walker R J and Bowen L 2011 Fault rocks from the SAFOD core samples: Implications for weakening at shallow depths along the San Andreas Fault, California; *J. Struct. Geol.* **33(2)** 132–144, https://doi.org/10.1016/j.jsg.2010.11.010.

Ikari M J, Saffer D M and Marone C 2009 Frictional and hydrologic properties of clayrich fault gouge; *J. Geophys. Res.* **114** B05409, https://doi.org/10.1029/2008JB006089.

Ismat Z and Mitra G 2001 Microfracturing associated with reactivated fault zones and shear zones; What can it tell us about deformation history ?; In: The nature and tectonic significance of fault zone weakening (ed.) Holdsworth Robert E, *Geol. Soc., Spec. Publ.* **186** 113–140.

Ito H and Kiguchi T 2005 Distribution and properties of fractures in and around the Nojima Fault in the Hirabayashi GSJ borehole; In: Petrophysical properties of crystalline rocks (eds) Harvey P K *et al.*, *Geol. Soc. Spec. Publ.* **240** 61–74, https://doi.org/10.1144/GSL.SP.2005.240.01.06.

Janssen C, Wirth R, Rybaoki E, Naumann R, Lemnitz H, Wenk H R and Dresen G 2010 Amorphous material in SAFOD core samples (San Andreas Fault): Evidence for crush-origin pseudotachylyte; *Geophys. Res. Lett.* **37** L01303, https://doi.org/10.1029/2009GL040993.

Janssen C, Wirth R, Wenk H R, Morales L, Naumann R, Kienast M, Song S R and Dresen G 2014 Faulting processes in active faults – Evidences from TCDP and SAFOD drill core samples; *J. Struct. Geol.* **65** 100–116, https://doi.org/10.1016/j.jsg.2014.04.004.

Jeppson T N and Tobin H J 2015 San Andreas Fault Zone velocity structure at SAFOD at core, log, and seismic scales; *J. Geophys. Res.: Solid Earth* **120** 4983–4997, https://doi.org/10.1002/2015JB012043.

Jeppson T N, Bradbury K K and Evans J P 2010 Geophysical properties within the San Andreas Fault Zone at the San Andreas Fault Observatory at Depth and their relationships to rock properties and fault zone structure; *J. Geophys. Res.* **115** B12423, https://doi.org/10.1029/2010JB007563.

Kaila K L, Reddy P R, Dixit M M and Lazarenko M A 1981 Deep crustal structure at Koyna, Maharashtra, indicated by deep seismic soundings; *J. Geol. Soc. India* **22** 1–16.

Kailasam L N, Reddi A G B, Joga Rao M V, Satyamurthy K, and Murthy B S R 1976 Deep electrical resistivity soundings in the Deccan Trap region; *Curr. Sci.* **45** 9–13.

Kanamori H and Brodsky E E 2004 The physics of earthquakes; *Rep. Progr. Phys.* **67** 1429–1496, https://doi.org/10.1088/0034-4885/67/8/R03.

Khadri S F R, Subbarao K V, Hooper P R and Walsh J N 1988 Stratigraphy of Thakurvadi formation, Western Deccan basalt province; *Geol. Soc. India Memoir* **10** 281–304.

Lachenbruch A H and Sass J H 1980 Heat flow and energetics of the San Andreas Fault Zone; *J. Geophys. Res. – Solid Earth* **85(B11)** 6185–6222, https://doi.org/10.1029/JB085iB11p06185.

Lin A 1996 Injection veins of crushing-originated pseudotachylyte and fault gouge formed during seismic faulting; *Eng. Geol.* **43** 213–224.

Lin A 2008 Fossil Earthquakes: The Formation and Preservation of Pseudotachylytes; *Lecture Notes in Earth Sciences*, Springer, Vol. **111**.

Lin A 2011 Seismic slip recorded by fluidized ultracataclastic veins formed in a coseismic shear zone during the 2008 Mw 7.9 Wenchuan earthquake; *Geology* **39(6)** 547–550, https://doi.org/10.1130/G32065.1.

Lin A and Nishiwaki T 2019 Repeated seismic slipping events recorded in a fault gouge zone: Evidence from the Nojima Fault drill holes, SW Japan; *Geophys. Res. Lett.* **46** 1276–1283, https://doi.org/10.1029/2019GL081927.

Lin A, Shimamoto T, Maruyama T, Sigetomi M, Miyata T, Takemura K, Tanaka H, Uda S and Murata A 2001 Comparative study of cataclastic rocks from a drill core and outcrops of the Nojima Fault zone on Awaji Island, Japan; *Island Arc* **10** 368–380, https://doi.org/10.1111/j.1440-1738.2001.00335.x.

Lin W, Yeh E C, Hung J H, Haimson B and Hirono T 2010 Localized rotation of principal stress around faults and fractures determined from borehole breakouts in hole B of the Taiwan Chelungpu-fault Drilling Project (TCDP); *Tectonophys.* **482** 82–91, https://doi.org/10.1016/j.tecto.2009.06.020.

Lin A, Mikako S, Yan B and Wang M 2015 Co-seismic surface ruptures produced by the 2014 M_w 6.2 Nagano earthquake, along the Itoigawa-Shizuoka Tectonic Line, central Japan; *Tectonophys.* **656** 142–153.

Lockner D A, Tanaka H and Ito H 2009 Geometry of the Nojima Fault at Nojima–Hirabayashi, Japan – I. A simple damage structure inferred from borehole core permeability; *Pure Appl. Geophys.* **166** 1649–1667, https://doi.org/10.1007/s00024-009-0515-0.

Lockner D A, Morrow C, Moore D and Hickman S 2011 Low strength of deep San Andreas fault gouge from SAFOD core; *Nature* **472** 82–86, https://doi.org/10.1038/nature09927.

Louis L, Chen T M N, David C, Robion P, Wong T F and Song S R 2008 Anisotropy of magnetic susceptibility and P-wave velocity in core samples from the Taiwan Chelungpu-Fault Drilling Project (TCDP); *J. Struct. Geol.* **30(8)** 948–962, https://doi.org/10.1016/j.jsg.2008.03.006.

Ma K F, Lee C T, Tasi Y B, Shin T C and Mori J 1999 The Chi-Chi Taiwan earthquake: Large surface displacements on inland thrust fault; *EOS Trans. AGU* **80** 605–611.

Ma K F, Mori J, Lee S J and Yu S B 2001 Spatial and temporal distribution of slip for 1999 Chi-Chi, Taiwan, earthquake; *Bull. Seismol. Soc. Am.* **91** 1069–1087.

Ma K F, Tanaka H and Song S R 2006 Slip zone and energetics of a large earthquake from the Taiwan Chelungpu-fault Drilling Project; *Nature* **444** 473–476, https://doi.org/10.1038/nature05253.

Mahoney J J 1988 Deccan traps; In: *Continental flood basalts* (ed.) Macdougall J D, Kluwer, Dordrecht, pp. 151–194.

Matin A and Misra S 2009 Repeated cataclasis in a reactivated fault zone – an example from Bengal Basin Margin Fault, Jharkhand, India; In: Geological Anatomy of India and the Middle East (eds) Talat Ahmad, Francis Hirsch, and Punya Charusiri, *J. Virtual Explorer* **32** 6.

McGarr A, Simpson D and Seeber L 2002 Case histories of induced and triggered seismicity; In: *International Handbook of Earthquake and Engineering Seismology* (eds) Lee W, Jenning P, Kisslinger C and Kanamori H, UK: Elsevier **81A** 647–661.

Misra S, Roy S, Bartakke V, Athavale G and Gupta H 2017 Fissures and fractures in the Koyna Seismogenic zone, western India; *J. Geol. Soc. India* **90** 131–137.

Mitchell C and Widdowson M 1991 A geological map of the southern Deccan Traps, India and its structural implications; *J. Geol. Soc.* **148** 495–505, https://doi.org/10.1144/gsjgs.148.3.0495.

Moore D and Lockner D 2013 Chemcial controls on fault behavior: Weakening of serpentinite sheared against quartz bearing rocks and its significance for fault creep in the San Andreas system; *J. Geophys. Res.* **118**, https://doi.org/10.1002/jgrb.50140.

Morgan W J 1972 Deep mantle convection plumes and plate motions; *Bull. Am. Assoc. Petrol. Geol.* **56** 203–213.

Najafi S, Cox K G and Sukeshwala R N 1981 Geology and geochemistry of the basalt flows, Deccan Traps, of the Mahad–Mahabaleshwar section, India; In: Volcanism and related provinces in other parts of the world (eds) Subbarao K V and Sukeshwala R N; *Geol. Soc. India Memoir* **3** 300–315.

Nielsen S, Di Toro G, Hirose T and Shimamoto T 2008 Frictional melt and seismic slip; *J. Geophys. Res.- Solid Earth* **B1** 113, https://doi.org/10.1029/2007JB005122.

Passchier C W and Trouw R A J 2005 *Micro-tectonics,* 2nd edn; Springer Berlin Heidelberg New York Press, 366p.

Podugu N, Mishra S, Wiersberg T and Roy S 2019 Chemical and noble gas isotope compositions of formation gases from a 3 km deep scientific borehole in the Koyna Seismogenic Zone, Western India; *Hindawi Geofluids*, Article ID 1078942, https://doi.org/10.1155/2019/1078942.

Rao B Y J, Sreenivas B, Kumar V T, Khadke N, Krishna A K and Babu E V S S K 2017 Evidence for Neoarchean Basement for the Deccan Volcanic flows around Koyna–Warna region, western India: Zircon U–Pb age and Hf-isotopic results; *J. Geol. Soc. India* **90** 752–760, https://doi.org/10.1007/s12594-017-0787-4.

Reches Z and Ito H 2007 Scientific drilling of active faults: Past and future; In: *Continental Scientific Drilling* (eds) Harms U, Koeberl C and Zoback M D, Springer, Berlin, Heidelberg, https://doi.org/10.1007/978-3-540-68778-8_6.

Rice J R 2006 Heating and weakening of faults during earthquake slip; *J. Geophys. Res.* **111** B05311, https://doi.org/10.1029/2005JB004006.

Roy S 2017 Scientific drilling in Koyna region, Maharashtra; *Curr. Sci.* **112** 11.

Roy S, Rao N P, Akkiraju V V, Goswami D, Sen M K, Gupta H, Bansal B K and Nayak S 2013 Granitic basement below Deccan Traps unearthed by drilling in the Koyna seismic zone, western India; *J. Geol. Soc. India* **81** 289–290.

Schleicher A M, Pluijm V D, Solum J G and Warr L N 2006 Origin and significance of clay-coated fractures in mudrock fragments of the SAFOD borehole (Parkfield, California); *Geophys. Res. Lett.* **33** L16313, https://doi.org/10.1029/2006GL026505.

Scholz C H 2002 *The mechanics of earthquakes and faulting*; Cambridge University Press, New York.

Scholz C H 2006 The strength of the San Andreas Fault: A critical analysis; *Geophys. Monogr. Ser.* **170**, https://doi.org/10.1029/170GM30.

Seth H C 1999 Flood basalts and large igneous provinces from deep mantle plumes: Fact, fiction, and fallacy; *Tectonophys.* **311** 1–29.

Seth H C 2007 Large Igneous Provinces (LIPs): Definition, recommended terminology, and a hierarchical classification; *Earth-Sci. Rev.* **85** 117–124, https://doi.org/10.1016/j.earscirev.2007.07.005.

Shashidhar D, Mallika K, Mahato C R, Maity B S and Satyanarayana H V S 2017 Recent seismicity patterns and microearthquake activity on an active intraplate fault system at Koyna-Warna, western India; *J. Geol. Soc. India* **90** 798–801, https://doi.org/10.1007/s12594-017-0794-5.

Sibson R H I973 Interactions between temperature and pore fluid pressure during earthquake faulting – a mechanism for partial or total stress relief; *Nature, Phys. Sci.* **243** 66–68, https://doi.org/10.1038/physci243066a0.

Sibson R H 1974 Frictional constraints on thrust, wrench and normal faults; *Nature* **249** 542–544, https://doi.org/10.1038/249542a0.

Sibson R H 1975 Generation of Pseudotachylyte by Ancient Seismic Faulting; *Geophys. J. Int.* **43(3)** 775–794, https://doi.org/10.1111/j.1365-246X.1975.tb06195.x.

Sibson R H 1977a Fault rocks and fault mechanisms; *J. Geol. Soc. London* **133** 191–213.

Sibson R H 1977b Kinetic shear resistance, fluid pressures and radiation efficiency during seismic faulting; *Pure Appl. Geophys.* **115** 387-400.

Sibson R H 1986a Earthquakes and rock deformation in crustal fault zones; *Ann. Rev. Earth Planet. Sci.* **14** 149–175, https://doi.org/10.1146/annurev.ea.14.050186.001053.

Sinha D K, Som A and Roy S 2017 The subsurface megascopic characteristics of basalt and basement rocks from Koyna Warna area of Maharashtra, India; *J. Geol. Soc. India* **90** 761–768.

Sutherland R, Toy V G, Townend J, Cox S C, Eccles J D, Faulkner D R, Prior D J, Norris R J, Mariani E, Boulton C, Carpenter B M, Menzies C D, Little T A, Hasting M, De Pascale G P, Langridge R M, Scott H R, Reid Lindroos Z, Fleming B and Kopf A J 2012 Drilling reveals fluid control on architecture and rupture of the Alpine fault, New Zealand; *Geology* **40(12)** 1143–1146, https://doi.org/10.1130/G33614.1.

Talwani P 1997a Seismotectonics of the Koyna–Warna area, India; *Pure Appl. Geophys.* **150** 511–550.

Talwani P 1997b On the nature of reservoir-induced seismicity; *Pure Appl. Geophys.* **150** 473–492.

Taylor B, Weiss J R, Goodliffe A M, Sachpazi M, Laigle M and Hirn A 2011 The structures, stratigraphy and evolution of the Gulf of Corinth rift, Greece; *Geophys. J. Int.* **185(3)** 1189–1219, https://doi.org/10.1111/j.1365-246X.2011.05014.x.

Townend J, Sutherland R, Toy V G, Eccles J D, Boulton C, Cox S C and McNamara D 2013 Late-interseismic state of a continental plate-bounding fault: Petrophysical results from DFDP-1 wireline logging and core analysis, Alpine Fault, New Zealand; *Geochem. Geophys. Geosyst.* **14** 3801–3820, https://doi.org/10.1002/ggge.20236.

Toy V G, Boulton C J, Sutherland R, Townend J, Norris R J, Little T A, Prior D J, Mariani E, Faulkner D, Menzies C D, Scott H and Carpenter B M 2015 Fault rock lithologies and architecture of the central Alpine fault, New Zealand, revealed by DFDP-1 drilling; *Lithosphere* **7(2)** 155–173, https://doi.org/10.1130/L395.1.

Toy V G *et al.* 2017 Bedrock geology of DFDP-2B, central Alpine Fault, New Zealand; *J. Geol. Geophys.* **60(4)** 497–518, https://doi.org/10.1080/00288306.2017.1375533.

Venkatesan T R, Pande K and Gopalan K 1986 ^{40}Ar/^{39}Ar dating of Deccan basalts; *J. Geol. Soc. India* **27** 102–109.

Vrolijk P, Ben A and Pluijm V D 1999 Clay gouge; *J. Struct. Geol.* **21(8-9)** 1039–1048, https://doi.org/10.1016/S0191-8141(99)00103-0.

Warr L N, Wojatschke J, Carpenter B M, Marone C, Schleicher A M, Ben A and Pluijm V 2014 A 'slice-and-view' (FIB–SEM) study of clay gouge from the SAFOD creeping section of the San Andreas Fault at ∼2.7 km depth; *J. Struct. Geol.* **69(A)** 234–244, https://doi.org/10.1016/j.jsg.2014.10.006.

Wdowinski S 1998 A theory of intraplate tectonics; *J. Geophys. Res.* **103** 5037–5059, https://doi.org/10.1029/97JB03390.

Wibberley C A J, Yielding G and Di Toro G 2008 Recent advancement in the understanding of fault zone internal structure: A review; *Geol. Soc. London, Spec. Publ.* **299** 5–33, https://doi.org/10.1144/SP299.2.

Wu H Y, Ma K F, Zoback M, Boness N, Ito H, Hung J H and Hickman S 2007 Stress orientations of TiwanChelungpu-Fault drilling project (TCDP) hole-A as observed from geophysical logs; *Geophys. Res. Lett.* **34** L01303, https://doi.org/10.1029/2006GL028050.

Wu Y H, Yeh E C, Dong J J, Kuo L W, Hsu J Y and Hung J H 2008 Core-log integration studies in hole-A of Taiwan Chelungpu-fault Drilling Project; *Geophys. J. Int.* **174(3)** 949–965, https://doi.org/10.1111/j.1365-246X.2008.03841.x.

Yeh E C, Sone H, Nakaya T, Ian K H, Song S R, Hung J H, Lin W, Hirono T, Wang C Y, Ma K F, Soh W and Kinoshita M 2007 Core description and characteristics of fault zones from hole-A of the Taiwan Chelungpu–Fault Drilling Project, https://doi.org/10.3319/TAO.2007.18.2.327(TCDP).

Zoback M L, Zoback M D, Adams J, Assumpcao M, Bell S, Bergman E A, Blumling P, Brereton N R, Denham D, Ding J, Fuchs K, Gay N, Gregersen S, Gupta H K, Gvishiani A, Jacob K, Klein R, Knoll P, Magee M, Mercier J L, Muller B C, Paquin C, Rajendran K, Stephansson O, Suarez G, Suter M, Udias A, Xu Z H and Zhizhin M 1989 Global patterns of tectonic stress; *Nature* **341** 291–298.

Zoback M, Hickman S and Ellsworth W 2010 Scientific drilling into the San Andreas fault zone; *EoS Trans. AGU* **91(22)** 197–199, https://doi.org/10.1029/2010EO220001.

Zoback M, Hickman S, Ellsworth W and Science Team SAFOD 2011 Scientific drilling into the San Andreas fault zone – An overview of SAFOD's first five years; *Scientific Drilling* **11** 14–28, https://doi.org/10.2204/iodp.sd.11.02.2011.

Zoback M D 2007 *Reservoir geomechanics*; Cambridge University Press.